

# Analysis of the Spatio-temporal Dynamics of COVID-19 in Massachusetts via Spectral Graph Wavelet Theory

Ru Geng, Yixian Gao, Hongkun Zhang, and Jian Zu

**Abstract**—The rapid spread of COVID-19 disease has had a significant impact on the world. In this paper, we study COVID-19 data interpretation and visualization using open-data sources for 351 cities and towns in Massachusetts from December 6, 2020 to September 25, 2021. Because cities are embedded in rather complex transportation networks, we construct the spatio-temporal dynamic graph model, in which the graph attention neural network is utilized as a deep learning method to learn the pandemic transition probability among major cities in Massachusetts. Using the spectral graph wavelet transform (SGWT), we process the COVID-19 data on the dynamic graph, which enables us to design effective tools to analyze and detect spatio-temporal patterns in the pandemic spreading. We design a new node classification method, which effectively identifies the anomaly cities based on spectral graph wavelet coefficients. It can assist administrations or public health organizations in monitoring the spread of the pandemic and developing preventive measures. Unlike most work focusing on the evolution of confirmed cases over time, we focus on the spatio-temporal patterns of pandemic evolution among cities. Through the data analysis and visualization, a better understanding of the epidemiological development at the city level is obtained and can be helpful with city-specific surveillance.

**Index Terms**—Spectral Graph Wavelet Transform, Graph Attention Neural Network, Graph Signal Processing, Spatio-temporal Dynamic Model, COVID-19.

## I. INTRODUCTION

WHEN writing this paper, the COVID-19 pandemic is still ongoing and has resulted in more than 260 million people diagnosed and more than 5 million deaths worldwide. The COVID-19 spreading was recognized by the World Health Organization (WHO) as a pandemic on March 11, 2020 [1]. As of December 1, 2021, confirmed cases in the United States surpassed 4,810,000 and Massachusetts surpassed 919,000 [2]. With little information on similar past pandemics, collecting mobility, safety, and behavior data related to COVID-19 and

learning from the collected data become the key for decision-makers. The final scale of the disaster had not yet been determined. To make matters worse, the mutation of the virus has led to waves of pandemics, and humankind still faces significant challenges.

Traditional mathematical models use compartmental models to study the transmission dynamics of COVID-19, such as SIR and SEIR models and their variants, see Gao et al. [3], Church [4], Neves and Guerrero [5], Ng and Gui [6]. Miranda et al. [7] construct a hybrid ODE-network model for the COVID-19 pandemic accounting for certain spatial aspects. Some state-of-the-art technologies, such as machine learning, and deep learning, have been introduced in the research of COVID-19. For example, Tang et al. [8] study the interplay of demographic variables and social distancing scores in the deep prediction of COVID-19 cases in the United States. Melin et al. [9] use a self-organizing mapping neural network to cluster countries with similar pandemics so that similar strategies can be used to deal with the spread of the virus. Tat Dat et al. [10] apply wavelet theory and machine learning method to study the evolution of the pandemic in France, Germany, Italy, the Czech Republic, and the US federal states of New York and Florida. Graphs and networks are used to model many real-world problems due to their flexible structure. Li and Mateos [11] conduct a graph Fourier frequency analysis to investigate the county-level contagion patterns of COVID-19. Gao et al. [12] utilize a new graph neural network – STAN to predict both state-level and county-level future number of infected cases. Kapoor et al. [13] examine COVID-19 forecasting using spatio-temporal graph neural networks. However, there is not much work analyzing the spatio-temporal pandemic spread patterns at the city levels.

In this paper, we focus on analyzing the local pandemic spread patterns in the State of Massachusetts (MA), USA, which covers a relatively small area of 21,000 square kilometers. Cars are the primary transportation tools among cities and towns in the state of MA. Therefore, the local spread of the pandemic is mainly affected by the transportation graph structure of the state. Unlike the state-level or county-level graphs mentioned above, our city-level graph is more suitable for the local epidemiological analysis in MA. In this Massachusetts Route Graph  $G_{MR} = (V, E)$ , hand-crafted from US Routes, we map cities to vertices on the graph, such that each vertex  $\tau_i \in V$  is associated with a set of time-dependent features extracted from biweekly COVID-19 data. The edge between two vertices represents that there is a

Manuscript received...

YX Gao is partially supported by NSFC grants (11871140, 12071065) and National Key R&D Program of China (2020YFA0714102). HK Zhang is partially supported by Simons Foundation Collaboration Grants for Mathematicians (706383). J Zu is partially supported by NSFC grants (11971096, 11971095). (Corresponding author: Jian Zu.)

Ru Geng, Yixian Gao and Jian Zu are with Center for Mathematics and Interdisciplinary Sciences, and School of Mathematics and Statistics, Northeast Normal University, Changchun, 130024, P.R. China (e-mail: zuj100@nenu.edu.cn).

Hongkun Zhang is with Department of Mathematics and Statistics, University of Massachusetts, Amherst MA 01003, US (e-mail: hongkun@math.umass.edu).

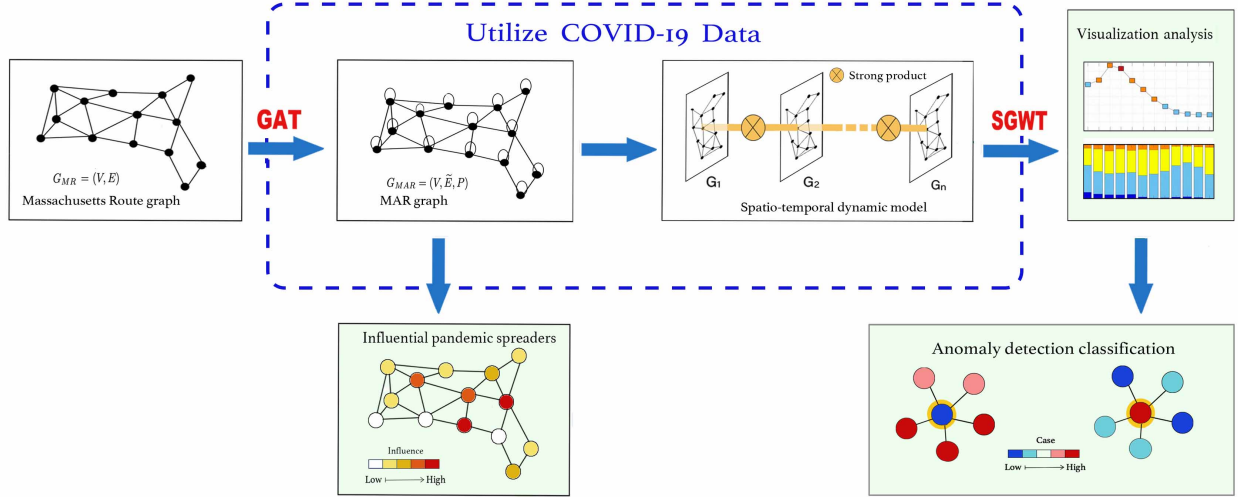


Fig. 1. The overall architecture of this paper.

US Route connecting the corresponding cities. The pandemic spreading between two cities may be affected not only by population movements such as transportation, commuting to work, and tourism; but also by hidden complex factors such as the circulation of COVID-19 virus-contaminated goods on the packaging, etc. Therefore, the traditional method of calculating the edge weight using distance and populations cannot accurately represent the pandemic spread among cities.

This paper further utilizes a deep learning method via graph neural networks – Graph Attention Network (GAT) – to learn the Markov transition matrix  $P$ , in order to capture geographical proximity and data features similarity in the transition probabilities. The resulting graph  $G_{MAR} = (V, \tilde{E}, P)$  is called the Massachusetts Attention Route (MAR) graph. GAT has been proved to be efficient for learning the edge weights by adaptive assigning different importance to different nodes through the learning of downstream tasks and data [14]–[19]. We also ranked the top influential cities for pandemic spread based on the attention coefficients learned from the GAT. Moreover, we construct the spatio-temporal dynamic graph model connected by the strong product [20].

To analyze the pandemic signals on the spatio-temporal dynamic graph model, we use a powerful tool – the spectral graph wavelet transform (SGWT). Indeed classical wavelet transformation has played an important role in multiresolution analysis, especially for studying signals containing discontinuities and sharp spikes. However, the construction of wavelets on graphs is rather difficult. Hammond et al. [21] and Shuman et al. [22] construct SGWT, and successfully apply it in studying graph signals and identifying anomalies. The SGWT coefficients contain rich information about the graph signal; however, it remains a big challenge to interpret them properly for non-experts. In this paper, we use a visualization methodology that relies on SGWT and the structure of our graph to enable the visual multiresolution analysis of time-varying COVID-19 data in Massachusetts. We analyze the dynamic patterns of pandemic signals for cities

and towns, and provide visualization diagrams based on our spectral graph wavelet analysis results. Moreover, we define an average metric function based on wavelet coefficients to give cities a spatio-temporal ranking synthetically. The top five ranked cities include Springfield, Amherst, Great Barrington, Holyoke, and Sandisfield, all in line with evidence of repeated poor responses to the pandemic, see [23]–[25]. For example, Amherst has reported pandemic peaks during the starting period of semesters of University of Massachusetts (UMass) Amherst, while Holyoke has reported pandemic breakout in its nursing homes. These all make the pandemic situation more severe than those in the surrounding areas. On the other hand, according to our ranking, we identify the five best-performance cities – New Marlborough, Harvard, West Tisbury, Tolland, and Leverett. These are in line with evidence showing their excellent pandemic prevention and control work, [26]–[29], which shows that the search for ambassadors at New Marlborough and the offer of free safety training courses in Harvard, make their pandemic situations much better than that of surrounding cities.

Experts often say that determining which cities and states have had the best response to COVID-19 thus far is tough and unfair [30]. In this paper we hope our study provides a useful evaluation method. The basic framework and main results of this paper are shown in Fig. 1.

In summary, the main contributions of this paper include:

- Massachusetts Route graph is constructed by connecting cities and towns based on US Routes or interstate highways.
- GAT learns the weights of the MAR graph, which helps calculate each node’s vulnerability affected by the COVID-19 infection rate of surrounding nodes.
- SGWT is used to analyze the spatio-temporal dynamic model constructed by the strong product.
- We design a new node classification method, which effectively identifies the anomaly cities based on spectral graph wavelet coefficients.

The outline of this paper is as follows: In section II, we describe the COVID-19 data of cities and towns in Massachusetts. In section III, we construct the Massachusetts Route graph and learn the pandemic transition probability Matrix by graph attention neural network, then build the spatio-temporal dynamic model of confirmed cases in Massachusetts. Section IV introduces the SGWT and develops the node classification method based on SGWT. In section V, we visually analyze the overall trend of the pandemic by SGWT, make a refined node classification in anomaly cities, and evaluate the city's pandemic prevention work. In addition, we identify the top influential pandemic spreader in the MAR graph. In section VI, we close with a conclusion section.

## II. COVID-19 DATA DESCRIPTION

This paper studies the COVID-19 pandemic spread in the state of Massachusetts, USA, which consists of 351 cities and towns. In the MA, the list of 10 largest cities (in population) is Boston (692,958), Worcester (191,575), Springfield (156,245), Lowell (116,143), Cambridge (111,989), Quincy (101,531), Lynn (100,824), New Bedford (99,980), Brockton (99,226) and Fall River (89,317). See Fig. 2 for the locations of these cities.

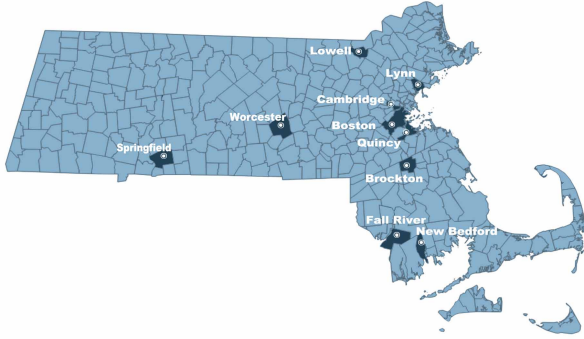


Fig. 2. Map of Massachusetts.

The dataset available in this paper is composed of population data  $\{N_i, i = 1, \dots, 351\}$  and the "two-week-case" time series data  $\{\gamma_i(t), t = 1, \dots, 41\}$  at the city/town level in Massachusetts, from December 6, 2020 to September 25, 2021, for 41 weeks total, which is collected from the official website [31]. We define the biweekly confirmed COVID-19 cases per thousand population (abbreviated as confirmed cases), denoted by the multivariate time series

$$\mathbf{x}_i(t) = 1000 * \frac{\gamma_i(t)}{N_i}, \quad i = 1, \dots, N, \quad t = 1, \dots, T \quad (1)$$

with  $N = 351$  and  $T = 41$ .

The multivariate time series data  $\mathbf{x}_i(t)$  will first be used to learn the pandemic transition probability  $p_{i,j}$  from city  $i$  to city  $j$ , in order to better capture the spatio-temporal evolution of the local pandemic spread dynamics. After that, their evolution patterns will be analyzed using the spatio-temporal dynamic graph model, and we are able to identify the most influential spreaders (cities), and detect anomaly cities with unusual pandemic spread patterns.

## III. MASSACHUSETTS ATTENTION ROUTE GRAPH AND SPATIO-TEMPORAL DYNAMIC MODEL

In this section, we first construct the Massachusetts Route graph  $G_{MR} = (V, E)$  based on US Routes, then learn the attention graph weight  $P$  from the COVID-19 data using GAT to get the Massachusetts Attention Route (MAR) Graph  $G_{MAR} = (V, \tilde{E}, P)$ . The strong product is utilized to construct a spatio-temporal dynamic graph model.

### A. Construction of the Massachusetts Route graph

We take the longitude and latitude coordinates of the cities and towns as the vertices  $\tau_i \in V$  from the website [32]. The detailed list of cities and their corresponding vertex ID is included in the Appendix. An edge  $e_{i,j} \in E$  represents the existing US Routes or interstate highways go through the administrative regions of the cities  $\tau_i, \tau_j \in V$  successively. We also connect the cities of Barnstable (No.21), Nantucket (No.197), and Oak Bluffs (No.221) because of the heavy sea transportation among them. The number of cities and towns in our study is  $|V| = N = 338^1$ . Let  $A \in \mathbb{R}^{N \times N}$  be the adjacency matrix of the graph  $G_{MR}$ , such that  $a_{i,j} = 1$  if  $e_{i,j} \in E$ , and  $a_{i,j} = 0$  otherwise. Each vertex has signals  $\mathbf{x}_i \in \mathbb{R}^T$ ,  $\gamma_i \in \mathbb{R}^T$  and  $N_i \in \mathbb{R}$  defined as in formula (1).

The size of vertices in Fig. 3 is proportional to the city population. For example, Vertex No. 36 represents metropolitan Boston, with the largest population in Massachusetts.

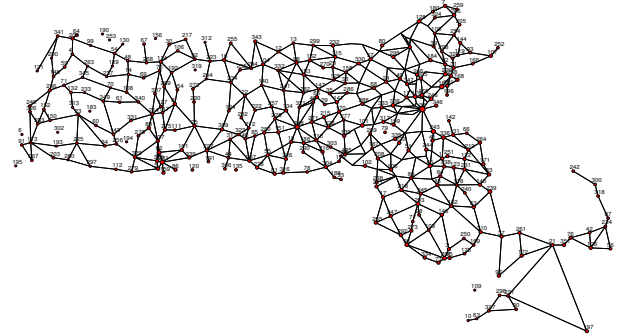


Fig. 3. Massachusetts Route graph  $G_{MR}$ .

Since the cities within the range between  $71^\circ\text{E}$  to  $71.5^\circ\text{E}$  and  $42^\circ\text{N}$  to  $42.8^\circ\text{N}$  are dense, to improve the visualization in Fig. 3, we use the downsampling method [33] by hiding some nodes in the Massachusetts Route graph. Specifically, we hide the nodes with negative signs in the nodal domain of the largest eigenvector of the Laplacian of the Massachusetts Route graph  $G_{MR}$ .

### B. Massachusetts Attention Route graph learned by graph neural network

The pandemic spreading between two cities may be affected by many complex factors, including transportation, tourism, commuting, and other hidden factors such as the circulation of

<sup>1</sup>There are 13 small towns located in rugged areas without any highway or heavy sea transportation. We do not consider them in our following study.

COVID-19 virus-contaminated goods. Due to the complexity of the pandemic, the traditional weighting method by distance is not a good choice in modeling the pandemic spread between cities (towns). In order to accurately capture the pandemic transition probabilities between cities, we utilize a deep learning method via GAT, to construct the transition probability matrix  $P = \{p_{ij}\}$ , based on the importance of geographical proximity on the Massachusetts Route graph  $G_{MR} = (V, E)$  and data feature similarity. The resulting new directed graph with self-loops is called the Massachusetts Attention Route (MAR) graph, denoted as  $G_{MAR} = (V, \tilde{E}, P)$ . The edge set  $\tilde{E}$  includes  $E$ , as well as self-loops.

GAT is a powerful deep learning method proposed in [14], which has state-of-the-art performance on node classification and link predictions. Instead of a simple mean aggregation, the GAT learns to use weighted summation to aggregate the features of neighboring nodes to update the features of the nodes, and automatically adjust the weight through downstream tasks [14]–[18]. Given  $N$  multivariate time series  $\mathbf{x}_i(t)$ , for  $i = 1, \dots, N$ ,  $t = 1, \dots, T$ . Then  $\mathbf{x}_i \in \mathbb{R}^T$  can be viewed as the  $T$ -dimensional input features of the node  $\tau_i$ . We use edge classification as the downstream task, for our GAT neural network, and use the normalized attention matrix in the last layer of the neural network as our Markov transition matrix  $P = \{p_{ij}\}$ .

To improve the model capacity and stabilize the learning process, GAT uses multi-head attention. Consider a multi-head GAT layer with  $K$  heads.  $\mathbf{W}^k \in \mathbb{R}^{O_k \times T}$ ,  $k = \{1, \dots, K\}$ , is a learnable linear transformation, with  $O_k \geq 1$ . Let  $\hat{\mathbf{a}}^k \in \mathbb{R}^{2O_k}$  be the  $k$ -th attention weight vector. The normalized attention coefficients  $\alpha_{ij}^k$  capture the importance of  $\tau_j$ 's features to  $\tau_i$ 's, expressed as

$$\alpha_{ij}^k = \frac{\exp\left(\text{LeakyReLU}(\hat{\mathbf{a}}^k \cdot [\mathbf{W}^k \mathbf{x}_i \parallel \mathbf{W}^k \mathbf{x}_j])\right)}{\sum_{l \in \mathcal{N}_i} \exp\left(\text{LeakyReLU}(\hat{\mathbf{a}}^k \cdot [\mathbf{W}^k \mathbf{x}_i \parallel \mathbf{W}^k \mathbf{x}_l])\right)}, \quad (2)$$

where  $\mathcal{N}_i$  denotes the set of first-order neighbours of node  $\tau_i$  (including  $\tau_i$ ) and  $\parallel$  denotes the concatenation operation, and the activation function is LeakyReLU<sup>2</sup>.

Let  $\mathbf{x}'_i \in \mathbb{R}^O$  be  $O$ -dimensional output features satisfying  $O = \sum_{k=1}^K O_k$ . A  $K$ -head GAT layer aggregates nodes features across neighborhoods by

$$\mathbf{x}'_i = \parallel_{k \in \{1, \dots, K\}} \text{ELU} \left( \sum_{j \in \mathcal{N}_i} \alpha_{ij}^k \mathbf{W}^k \mathbf{x}_j \right).$$

where ELU is an exponential linear unit<sup>3</sup>.

To learn the attention matrix, we use edge classification [15] as a downstream task. Let

$$M = \{(\tau_i, \tau_j) \in V \times V \mid a_{i,j} = 1\}$$

be the positive sample set, where  $a_{i,j}$  is the element of the adjacency matrix  $A$  of the graph  $G_{MR}$ . For any integer  $l \geq 1$ ,

the power of the adjacency matrix  $A^l = (a_{i,j}^{(l)})_{N \times N}$  can be used to define the  $l$ -th order neighborhood of a vertex. Let

$$S^- = \{(\tau_i, \tau_j) \in V \times V \mid a_{i,j} = 0, a_{i,j}^{(l)} > 0, \exists l \in \{2, 3\}\}$$

be the negative candidates set. The negative sample set  $M^-$  is randomly generated from the negative instances in  $S^-$  with a similar size to  $M$ . The GAT neural network is trained by minimizing the following cost function:

$$\mathcal{L} = - \frac{\sum_{(i,j) \in M \cup M^-} (a_{i,j} \log q_{ij} + (1 - a_{i,j}) \log(1 - q_{ij}))}{|M \cup M^-|}$$

Here  $q_{ij}$  is the probability of whether there is an edge between  $\tau_i$  and  $\tau_j$ ,

$$q_{ij} = \frac{1}{1 + \exp\left(-(\mathbf{x}''_i \odot \mathbf{x}''_j) \cdot \theta\right)},$$

where  $\odot$  denotes Hadamard product,  $\mathbf{x}''_i$  is the output feature of the last layer of GAT.  $\theta$  is a learned parameter vector and the dimension is the same as  $\mathbf{x}''_i$ .

In our setup, there are two GAT layers. Each layer takes an appropriate output dimensionality to improve the performance of the model [34]. The first layer is a  $K$ -head attention layer with  $K = 7$ , and the input feature is the graph signal  $\mathbf{x}_i \in \mathbb{R}^T$  with  $T = 41$ . The output feature  $\mathbf{x}'_i$  is cascaded as  $O = 854$ , i.e. we set  $O_k = 122$  features each (for a total of 854 features). The second layer is a single-head attention layer with the 88-dimensional output features  $\mathbf{x}''_i$ . During the training phase, we divide the sample set  $M \cup M^-$  into training set, validation set and test set according to the ratio of 6 : 2 : 2. We also make sure to keep the same number of positive and negative samples in the test set. The learning rate is set as  $lr = 0.005$ . The early stopping strategy is applied to the validation set to avoid overfitting, with the patience set to 100 epochs. **The accuracy of edge classification of  $G_{MR}$  without self-loops in our result is 0.9499.**

The transition probability  $p_{ij}$  is defined as the GAT coefficients of the last GAT layer, i.e.

$$p_{ij} = \frac{\exp\left(\text{LeakyReLU}(\hat{\mathbf{a}} \cdot [\mathbf{W} \mathbf{x}'_i \parallel \mathbf{W} \mathbf{x}'_j])\right)}{\sum_{l \in \mathcal{N}_i} \exp\left(\text{LeakyReLU}(\hat{\mathbf{a}} \cdot [\mathbf{W} \mathbf{x}'_i \parallel \mathbf{W} \mathbf{x}'_l])\right)},$$

where  $\hat{\mathbf{a}}$  and  $\mathbf{W}$  defined above are the learned attention weight vector and the learned parameter matrix of this single-head attention layer. One advantage is that the self-attention coefficient  $p_{i,i} > 0$ , which also explains the self-influence of the pandemic in a city. Consequently, the obtained MAR graph is a graph with self-loops. Fig. 4 shows the basic framework of this method.

### C. Spatio-temporal dynamic graph model

To perform the spatio-temporal node classification using the time-dependent data  $\{\mathbf{x}_i(t), i = 1, \dots, N, t = 1, \dots, T\}$  defined in (1), we introduce the concept of graph product. The three well-known graph products are the graph Cartesian product, graph Kronecker product, and graph strong product, see Fig. 5. These have been powerful in studying time-vary data on graphs, see [35]–[38].

<sup>2</sup>LeakyReLU( $x$ ) = 0.35 $x(1 - \text{sgn}(x))/2 + x(1 + \text{sgn}(x))/2$ .

<sup>3</sup>ELU( $x$ ) = ( $\exp(x) - 1$ )( $1 - \text{sgn}(x)$ )/2 +  $x(1 + \text{sgn}(x))/2$ .

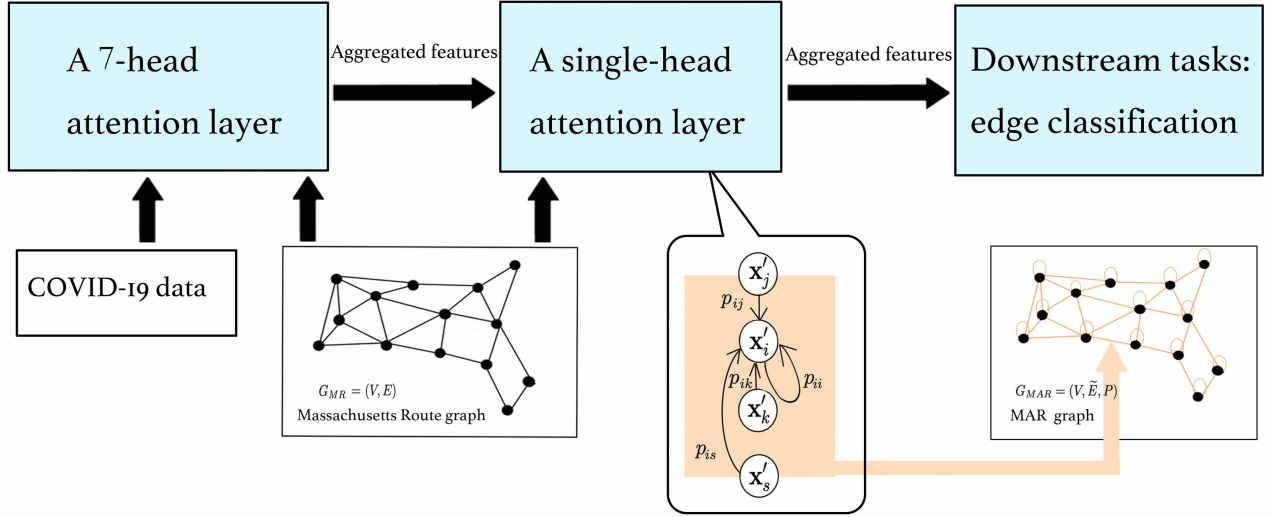


Fig. 4. GAT framework with edge classification as a downstream task. There are two GAT layers. The first layer is a 7-head attention layer, and the second layer is a single-head attention layer. The attention coefficient learned by the GAT neural network is applied to define the MAR graph.

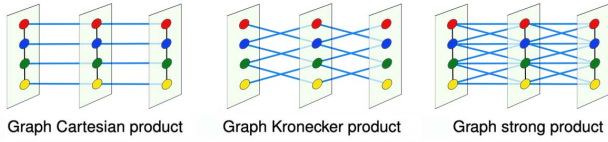


Fig. 5. Graph products of a spatial path graph (of 4 nodes) and a temporal path graph (of length 3).

The graph Cartesian product only adds extra edges between nodes on the adjacent graph time slices in series, which often weakens the influence of spatial neighbors in the study of SGWT for graph signals. Here we adapt the graph strong product, which also adds temporal edges between pairs of one-hop neighbors in its adjacent graph time slice.

Let  $H$  be a path graph consisting of  $T$  nodes. The strong product graph can be defined by the product of the Massachusetts Route graph  $G_{MR}$  and the path graph  $H$ . We assign weights to the strong product graph based on the transition probability matrix  $P$  of  $G_{MAR}$ . The resulting directed graph  $\mathcal{G}$  without self-loops is the spatio-temporal dynamic model. More precisely, the graph time slices  $\{G_t = (V_t, E_t, P_t), t = 1, \dots, T\}$  are copies of graph  $G_{MR}$  by assigning weights  $P_t = P - \text{diag}(p_{11}, p_{22}, \dots, p_{NN})$ . The direction of the temporal edge (black edge in Fig. 6) is from  $G_t$  to  $G_{t+1}$ , which represents the time-evolution of the pandemic among these cities. The weights of the new temporal edges are carried from  $P$ . Now, the strong product graph can be represented as  $\mathcal{G} = (\mathcal{V}, \mathcal{E}, \mathcal{W})$  with  $\mathcal{V} = \{\tau_{i,t}, i = 1, \dots, N; t = 1, \dots, T\}$ , and  $\mathcal{E} = (E_1 \cup \dots \cup E_T) \cup (E_{1,2} \cup \dots \cup E_{T-1,T})$ , where  $E_{t,t+1}$  is the collection of temporal edges connecting  $G_t$  and  $G_{t+1}$ . The new weight matrix  $\mathcal{W}$  is not normalized anymore, as we have added extra temporal edges, which carry the same weight as the spatial edges. More precisely, the edge  $(\tau_{i,t}, \tau_{j,t+1})$  has the same weight  $p_{ji}$  as the spatial edge  $(\tau_{i,t}, \tau_{j,t})$ , see Fig.

6. Note that  $\mathcal{W}$  is rather sparse, as we only added temporal edges between two adjacent graph time slices.

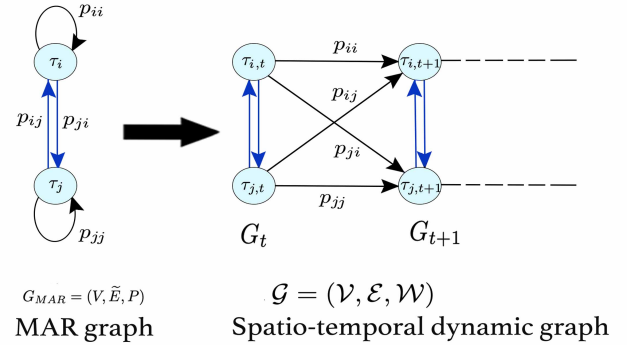


Fig. 6. Construction of spatio-temporal dynamic graph based on MAR graph. The black edge in the spatio-temporal dynamic graph represents the temporal edge, and the blue edge is the spatial edge inherited from the MAR graph without the self-loop.

#### IV. NODE CLASSIFICATIONS ON THE SPATIO-TEMPORAL DYNAMIC GRAPH $\mathcal{G}$

##### A. Brief introduction to the Spectral Graph Wavelet Transform

Let  $\mathcal{G} = (\mathcal{V}, \mathcal{E}, \mathcal{W})$  be the spatio-temporal graph constructed in the above section. The graph signal  $\mathbf{X}$  on  $\mathcal{V}$  with  $\mathbf{X}(\tau_{i,t}) = x_i(t)$  defined on (1) represents the confirmed cases of city  $i$  in the  $t$ -th week. Clearly, the cardinality of  $|\mathcal{V}| = \hat{N} := NT$ . The graph Laplacian is defined by  $\mathcal{L} = D - \mathcal{W}$ , where the degree matrix  $D = (d_{ii})$  is a diagonal matrix with entries  $d_{ii} = \sum_k w_{ik}$ . The graph Laplacian  $\mathcal{L}$  is not symmetric as our pandemic graph is directed. We construct a symmetric matrix by  $L = (\mathcal{L} + \mathcal{L}^*)/2$ , which is the averaging of the graph Laplacian and its transpose.  $L$  has  $\hat{N}$  non-negative, real-valued eigenvalues  $\Lambda = \{\lambda_1, \lambda_2, \dots, \lambda_{\hat{N}}\}$  with  $\lambda_1 = 0$ , and the



corresponding normalized eigenvectors  $\{\mathbf{u}_l, l = 1, \dots, \hat{N}\}$  form an orthonormal basis for the Hilbert space. The graph Fourier transformation of  $\mathbf{X}$  can be written as

$$\hat{\mathbf{X}}(\lambda_l) = \sum_{\tau \in \mathcal{V}} \mathbf{X}(\tau) \mathbf{u}_l(\tau).$$

A *graph spectral filter*, or *kernel*  $\hat{g} : \Lambda \rightarrow \mathbb{R}$  is a function defined in the spectral domain  $\lambda_l \in \Lambda$ . A *dictionary*  $\{\hat{g}_m\}_{m=1,2,\dots,M}$  is a set of graph spectral filters constructed to detect different frequencies of signals.

In this paper, we use the dictionary constructed by Hammond et al. [21]:

$$\{\hat{h}(\lambda), \hat{g}(s_{M-1}\lambda), \hat{g}(s_{M-2}\lambda), \dots, \hat{g}(s_1\lambda)\}, \quad (3)$$

where the wavelet kernel

$$\hat{g}(\lambda) = \begin{cases} \lambda^2, & 0 \leq \lambda < 1, \\ -5 + 11\lambda - 6\lambda^2 + \lambda^3, & 1 \leq \lambda \leq 2, \\ 4\lambda^{-2}, & \lambda > 2 \end{cases}$$

is a bandpass filter defined on the Fourier domain, the stretching scale  $s_1, s_2, \dots, s_{M-1}$  are logarithmically sampled between  $s_1 = 1/\lambda_{\hat{N}}$  and  $s_{M-1} = 40/\lambda_{\hat{N}}$ , the scaling function  $\hat{h}(\lambda) = b \exp\left(-\left(\frac{10\lambda}{0.3\lambda_{\hat{N}}}\right)^4\right)$  is a low-pass filter detecting the low frequency signal with the parameter  $b = \max_{\lambda} \hat{g}(\lambda)$ . Such dictionary is designed to evenly cover the graph spectrum domain.

Given a graph signal  $\mathbf{X}$  and the dictionary  $\{\hat{g}_m\}_{m=1,2,\dots,M}$ , the spectral graph wavelet coefficient  $W_{\mathbf{X}} : \{1, \dots, M\} \times \mathcal{V} \rightarrow \mathbb{R}$  is defined as

$$W_{\mathbf{X}}(m, \tau) = \sum_{l=1}^{\hat{N}} \hat{g}_m(\lambda_l) \hat{\mathbf{X}}(\lambda_l) \mathbf{u}_l(\tau). \quad (4)$$

However, the above SGWT is rather expensive for large graphs, as the resulting computational complexity is of order  $O(\hat{N}^3)$ . In this paper, we apply the fast spectral graph wavelet proposed in [21] to overcome this difficulty. The fast spectral graph wavelet transform based on Chebyshev polynomials approximation [39] shows that the graph wavelet coefficients in (4) can be approximated by

$$W_{\mathbf{X}}(m, \tau) \approx \left( \frac{1}{2} c_{m,0} \mathbf{X} + \sum_{k=1}^{K_m} c_{m,k} \bar{T}_k(L) \mathbf{X} \right) (\tau), \quad (5)$$

where  $K_m$  is the number of truncating terms, and

$$c_{m,k} = \frac{2}{\pi} \int_0^\pi \cos(k\theta) \hat{g}_m(\cos(\theta)) d\theta.$$

Moreover,  $\bar{T}_k$  is the shifted Chebyshev polynomials with the domain of  $[0, \lambda_{\hat{N}}]$ , such that  $\bar{T}_k(x)$  satisfies the recursive formula

$$\bar{T}_k(x) = \left( \frac{4}{\lambda_{\hat{N}}} x - 2 \right) \bar{T}_{k-1}(x) - \bar{T}_{k-2}(x),$$

with initial conditions

$$\bar{T}_0(x) = 1, \quad \bar{T}_1(x) = \frac{2}{\lambda_{\hat{N}}} x - 1.$$

The computational cost to approximate the wavelet coefficients is order  $O(K_m|\mathcal{E}| + K_m|\mathcal{V}|)$ .

In this paper, we take  $K_m = 40$  in (5). It takes 0.5 seconds on a laptop with a 2.3 GHz 8-core Intel Core i9 processor. Without Chebyshev approximation, it costs 650 seconds.

### B. Node Classification Using SGWT coefficients

Given our spatio-temporal dynamic graph  $\mathcal{G} = (\mathcal{V}, \mathcal{E}, \mathcal{W})$  together with the COVID-19 confirmed cases  $\mathbf{X}$ , one question is how to provide a high-quality classification of nodes according to the pandemic spreading patterns? We refer to this as the "node labeling problem" with the understanding that the node classification problem can be abstracted as providing a classification label for the graph structure. Here we will use the information already encoded in the SGWT coefficients to help us predict labels.

Let  $T = 41$  be the number of time slices in the spatio-temporal dynamic model from December 6, 2020, to September 25, 2021. Let  $M = 8$  be the number of graph spectral filters. Using the SGWT on the graph signal  $\mathbf{X}$ , one gets a  $\hat{N} \times M$  wavelet coefficient matrix with entries (5). We then define node classification criteria based on the multiresolution information carried by SGWT coefficients. We will classify the nodes by the torque value obtained by some weighted average of the SGWT coefficients.

#### Step 1: Data processing of wavelet coefficients.

Firstly, we use a data scaling method to ensure for each wavelet coefficient that guarantees that they are on the same scale. This method was introduced by RobustScaler [40] in the machine learning library Scikit-learn as follows:

$$S(m, \tau) = |W_{\mathbf{X}}(m, \tau)| / R(m),$$

where  $R(m)$  is the interquartile range of  $|W_{\mathbf{X}}(m, \tau)|$  with respect to  $\tau$ . The interquartile range is the difference between the first and third quartile of a data set. The quartiles make the RobustScaler ignore data points that are very different from the rest (like machine errors).

Secondly, we use logarithmic normalization to normalize each coefficient to  $[0, 1]$  to facilitate the calculation of the torque value and comparison,

$$\bar{W}_{\mathbf{X}}(m, \tau) = \frac{\ln(1 + S(m, \tau))}{\ln(1 + \max_{\tau} S(m, \tau))}.$$

Logarithmic normalization does not change the order of the values, but it can significantly reduce the effect of maximum abnormal value [41].

#### Step 2: Spatial node classifications based on torque values.

In order to use the SGWT coefficients to classify the nodes, we need to define the torque value function  $\varphi : \mathcal{V} \rightarrow \mathbb{R}$  by:

$$\varphi(\tau) = [\bar{W}_{\mathbf{X}}(1, \tau), \dots, \bar{W}_{\mathbf{X}}(8, \tau)] \cdot [-4, -3, -2, -1, 1, 2, 3, 4].$$

High torque values imply a high frequency of signal changes [38]. More precisely, if a vertex  $\tau(i, t)$  has a relatively high torque value, then there are anomalies in the pandemic spread patterns of the  $i$ -th city compared to its surrounding cities at the time  $t$ .

Let  $d = \max_{\tau} \varphi(\tau) - \min_{\tau} \varphi(\tau)$ . By splitting the interval  $[\varphi_{\min}, \varphi_{\max}]$  into 5 equal intervals, the vertex space  $\mathcal{V}$  can be divided into five disjoint sets  $\{\mathcal{V}_1, \mathcal{V}_2, \mathcal{V}_3, \mathcal{V}_4, \mathcal{V}_5\}$ , which

represent the spatio-temporal changes of the  $\mathbf{x}_i(t)$  (in terms of the SGWT coefficients) as low frequency, mid-low frequency, uncertain, mid-high frequency, and high frequency, respectively. The detailed node classifications are defined in Table I.

TABLE I  
NODE CLASSIFICATION IN  $\mathcal{V}$ .

Torque Value Range	$[\varphi_{\min}, d/5]$	$(d/5, 2d/5]$	$(2d/5, 3d/5]$	$(3d/5, 4d/5]$	$(4d/5, \varphi_{\max}]$
Node Subset	$\mathcal{V}_1$	$\mathcal{V}_2$	$\mathcal{V}_3$	$\mathcal{V}_4$	$\mathcal{V}_5$
Signal Frequency	low	mid-low	uncertainty	mid-high	high

The spatial node classification method is demonstrated in Fig. 7, for the 2-week period of Jan.31-Feb. 13, 2021.

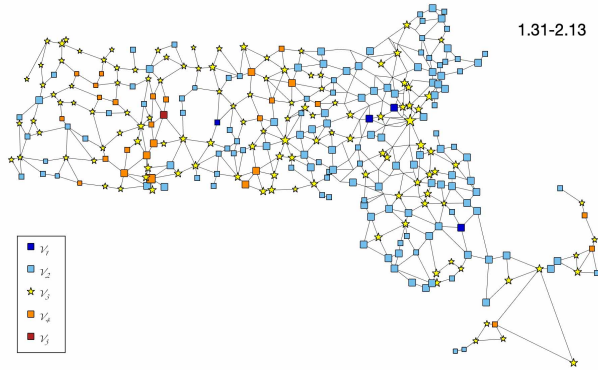


Fig. 7. Nodes classification of the 9th time slice. The dark red square represents Amherst.

An efficient node classification should be able to capture the abrupt changes of the graph signal, both spatially and temporally. To make the illustrations more explicit, we use our node classification method to investigate the city of Amherst during the 13 weeks from December 16, 2020, to March 13, 2021. Fig. 8 shows that the confirmed cases in Amherst were significantly higher than its neighbors from January 24, 2021 to February 27, 2021. Fig. 9 demonstrates the different temporal stages of the node classification value of Amherst during the 13 weeks. Compared with Fig. 8, we can see that when the City of Amherst has similar pandemic patterns as the surrounding cities, the wavelet coefficient represents low frequency (Dec. 6-Dec. 19). On the other hand, as the confirmed cases in the surrounding cities start to rise, the wavelet coefficient of Amherst represents high frequency (Dec. 20-Jan. 2), which means that the pandemic cases of Amherst have different patterns than its neighbors. Our node classification method accurately captures the abnormal pandemic spread patterns of Amherst during the period from January 24, 2021, to March 6, 2021, see Fig. 8 and Fig. 9. In this period, the University of Massachusetts Amherst partially opened its campus, and many students returned to Amherst [42].

This method can effectively identify the pandemic spread anomaly patterns of any specific period, which should be valuable for further research.

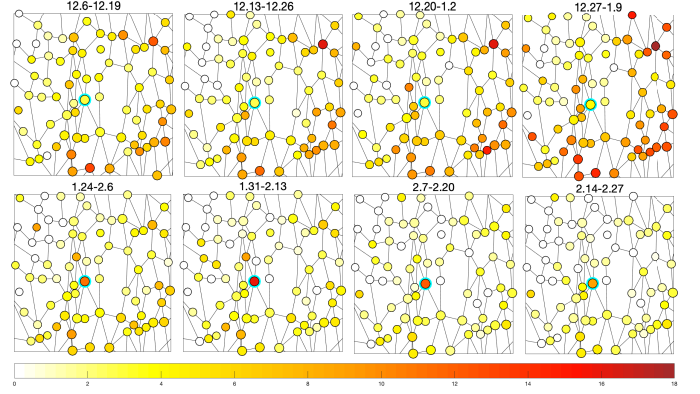


Fig. 8. Visualization of the pandemic graph signal  $\mathbf{X}$  at Amherst and its adjacent areas from Dec. 6, 2020, to Jan. 9, 2021 and Jan. 24, 2021, to Feb. 27, 2021. The color represents the actual value of the signal. The nodes marked by the blue circle represent the city of Amherst.

## V. VISUALIZATION ANALYSIS OF COVID-19 PANDEMIC SPREAD PATTERNS

In this section, we focus on the visualization analysis of the COVID-19 pandemic spread patterns on the spatio-temporal dynamic graph model. We first conduct an overall analysis of the COVID-19 data in Massachusetts. Then we identify the supper pandemic spreaders (cities). Finally, a refined node classification is performed in  $\mathcal{V}_4$  and  $\mathcal{V}_5$ , where the pandemic spread patterns have abrupt spatio-temporal changes.

### A. Overall graph classifications

To have an overall temporal analysis of the pandemic evolution patterns for cities in Massachusetts, we define a graph classification method for the spatio-temporal dynamic graph  $\mathcal{G}$ , which enables us to classify each graph time slice for  $\{G_t, t = 1, \dots, T\}$ .

First, we need to calculate the node classification distribution in  $G_t$ , which can be obtained by counting the frequencies of nodes in  $G_t$  that occur in each of the five classes  $\mathcal{V}_j$ ,  $j = 1, \dots, 5$ :

$$\sigma_t^j = \frac{1}{N} \sum_{i=1}^N \mathbb{I}_{\mathcal{V}_j}(\tau_{i,t}), j = 1, 2, \dots, 5, \quad (6)$$

where  $\mathbb{I}_{\mathcal{V}_j}$  is the indicator function of the set  $\mathcal{V}_j$ . The distribution  $\{\sigma_t^j, j = 1, \dots, 5\}$  can not be used to directly classify the graph  $G_t$ , as one has to weigh in the distributions in other time slices to well capture the role of each frequency class. We adopt the method used by Dal Col. etc. [38], by first taking  $\sigma_{\max}^j = \max\{\sigma_1^j, \sigma_2^j, \dots, \sigma_T^j\}$ . Then we define the class of  $G_t$  as  $\mathcal{V}_{r_t}$ , with

$$r_t = \arg \max_{j \in \{1, 2, 3, 4, 5\}} (\sigma_t^j / \sigma_{\max}^j). \quad (7)$$

Next we conduct a temporal graph classification to get an overall visual analysis of the spatio-temporal pandemic spread patterns in Massachusetts, which is demonstrated in Fig. 10. As we can see from Fig. 10, after Thanksgiving, 2021, Massachusetts saw a substantial spike in confirmed cases as there were more group gatherings. The confirmed cases in

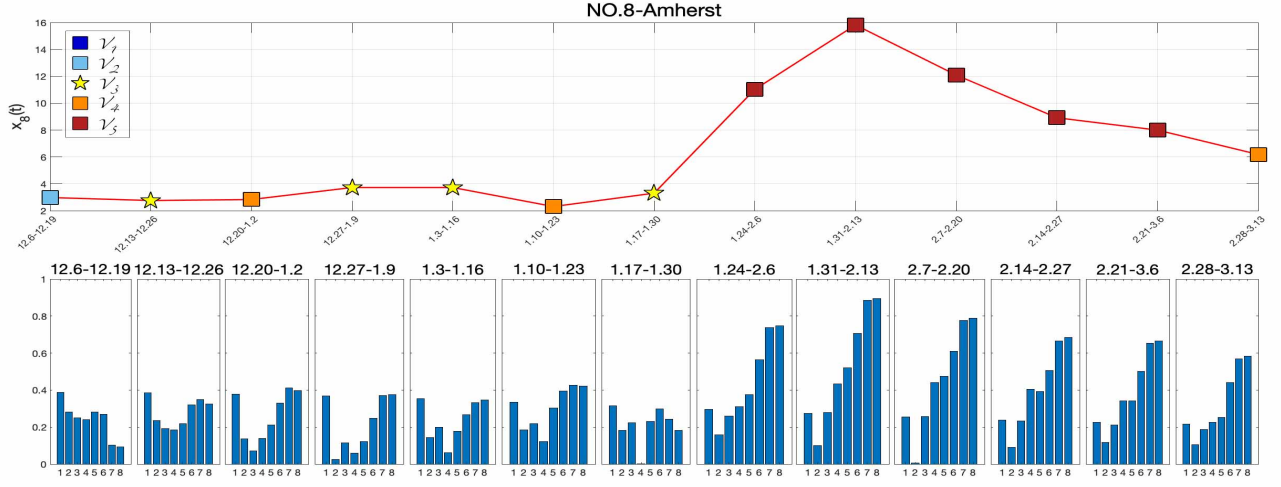


Fig. 9. Nodes classification (top) and normalized graph wavelet coefficients (bottom).

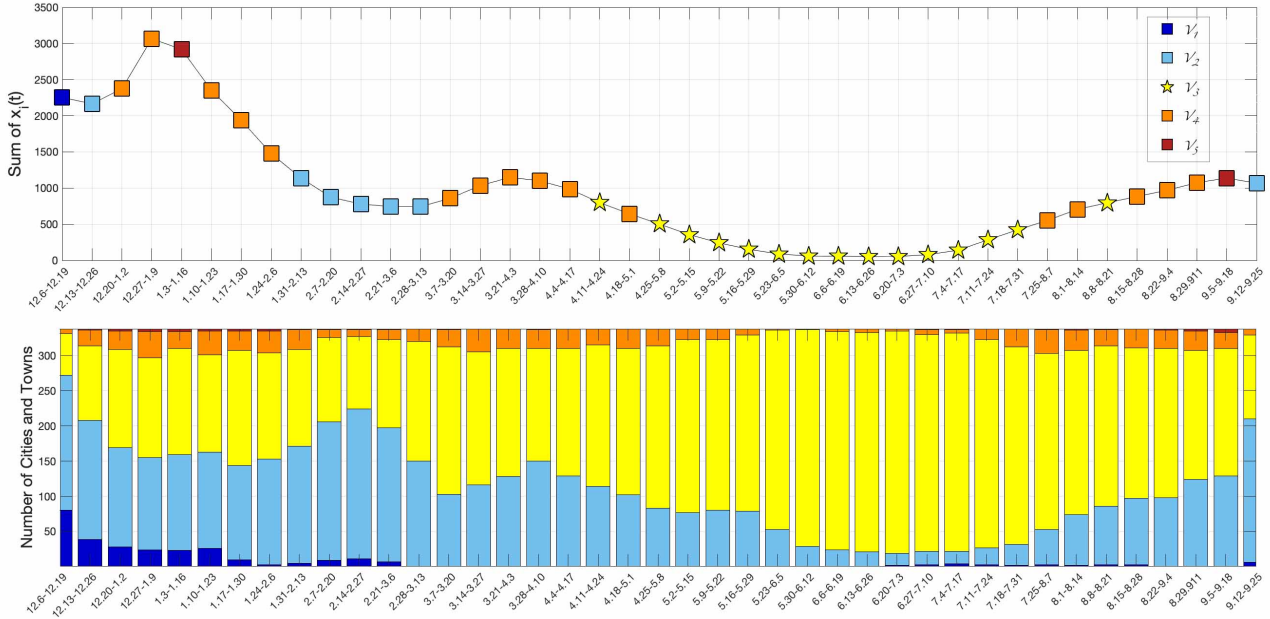


Fig. 10. Overall visual analysis of COVID-19 in Massachusetts. The figures depict graph classification for each graph time slice (**top**) using method (7), and the spatial node classification distribution  $\sigma_i^j$  given by (6) (**bottom**).

Massachusetts reached their peak during the Christmas holiday period. We can infer that multi-site outbreak patterns exist because the temporal and spatial changes of confirmed cases in many cities are different from those in the surrounding cities. The cases declined sharply after mid-January due to restricting gatherings, maintaining social distance, and advocating masks, then stabilized in late February (mid-low frequency). Massachusetts entered the fourth phase of the state's reopening plan on March 22, 2021. With the relaxation of pandemic restrictions, there was a small-scale rebound of confirmed cases with the multi-point pattern at the end of March (mid-high frequency). The numbers began to decrease from April to July due to the increased vaccination rate.

### B. Spatial ranking for super-spreader cities

Identifying influential spreaders (cities) in a pandemic network is a core question to prevent pandemic spreading. Many different centrality measures tied to the network topology have been introduced to find the central nodes. However, the importance of node features is mostly ignored in these works. The centrality of a node in a pandemic network should depend on two features: its local influence on the nodes in its one-hop neighbor and its global influence on the nodes belonging to higher-order hop neighbors. Taking advantage of the attention coefficients learned from the GAT, we introduce a new score function that allows us to redefine the classical centrality measure by considering their importance to the neighbors' features.

Considering the  $m$ -hop neighbor of node  $\tau_i$  in the MAR



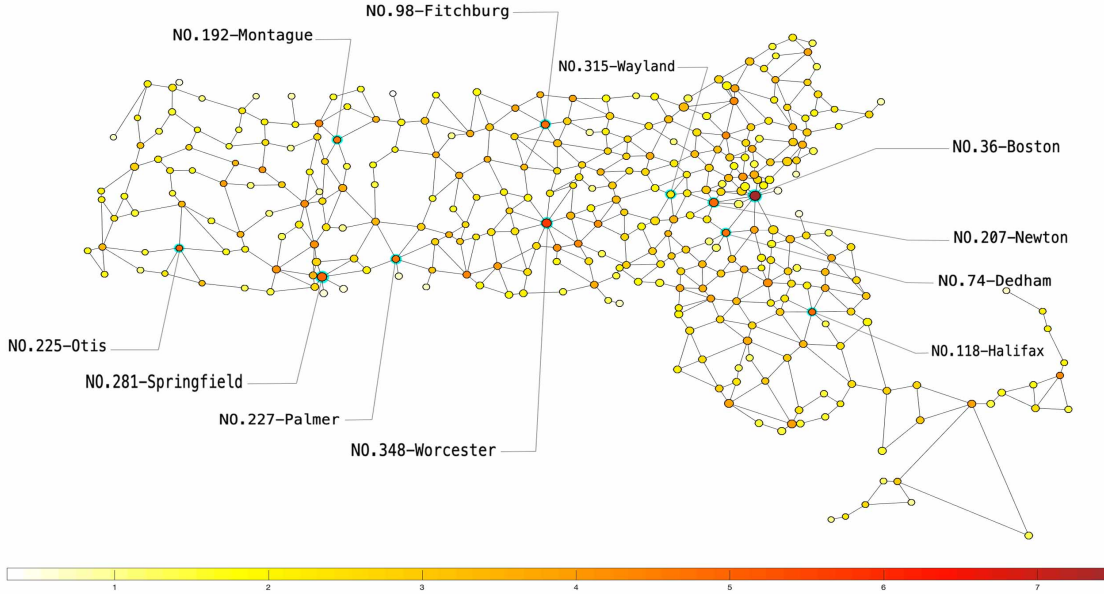


Fig. 11. City spatial ranking of pandemic spread capability: from dark red (top rank) to white (low rank).

graph  $G_{MAR} = (V, \tilde{E}, P)$ . The attention coefficient measures the importance of  $\tau_i$ 's features to  $\tau_j$ . Let  $P^m = (p_{i,j}^{(m)})_{N \times N}$  be the  $m$ -th power of the matrix  $P$ . Then  $p_{i,j}^{(m)}$  characterizes the  $m$ -step influence of city  $i$  to city  $j$ . We define a new centrality metric to capture the capability of city  $i$  to spread the pandemic to their neighbors by

$$c_i^{(m)} = \sum_j p_{ji}^{(m)}, j \neq i, m = 1, 2, 3, \dots$$

In our practice, we define the *influential score* of city  $i$  by

$$C_i = \sum_{m=1}^5 c_i^{(m)}$$

as the total capability of city  $i$  to spread the virus to other cities.

The spatial ranking of cities according to their influential scores is shown in Fig. 11. One can see that the top ten cities with the largest pandemic spread (influential) scores (in dark red) are Boston, Worcester, Springfield, Otis, Fitchburg, Newton, Halifax, Dedham, Montague and Palmer. It's not surprising that Boston, Worcester, and Springfield are in the top three, given these cities' large populations and high mobility. On the other hand, we are able to identify small cities, which are otherwise difficult to identify without using our advanced methods. For example, the City of Otis has a small population but ranked fourth on the list. It is remarkable that the City of Wayland has a larger population and the same number of connected US Routes compared to Otis, but it ranks much lower. This has been confirmed by news in [43], as well as the fact that Otis has a ski resort. Using this new ranking metric, we can correctly identify cities at risk and those more volatile to pandemics and thus need to invest more social resources to better control the pandemic.

### C. Refined node classification in anomaly cities

Given the COVID-19 data in Massachusetts, another important question is to identify cities with anomaly spread patterns during the pandemic period. More precisely, this is equivalent to finding patterns in data (i.e., attribute values or changes in the values over time) that are significantly different from that of the spatio-temporal neighbors. These non-conforming patterns are often referred to as anomalies. The typical anomaly detection method concentrates on time series, or static graph signals, which could not be applied to our case. We aim to design a new method that enables us to detect anomalies in COVID-19 time-series data belonging to multiple entities (cities) and explain the anomalies to domain experts in a comprehensible manner.

SGWT is a powerful tool for finding anomalies for spatio-temporal graph signals. For example, the set  $\mathcal{V}_5$  can be counted as one anomaly class, both spatially and temporally. However, in  $\mathcal{V}_5$ , by examining the distribution of the SGWT coefficients more carefully, we find that there are situations in which there is a node with a higher or lower signal value than that of the surroundings. As shown in Fig. 12, there are two dramatically types of vertices in  $\mathcal{V}_5$ , as indicated above.

Below we say the nodes in  $\mathcal{V}_4 \cup \mathcal{V}_5$  are anomaly nodes. The corresponding city is the anomaly city. We use a refined node classification method to identify these two abnormal situations in anomaly cities. Let  $\mathcal{N}_i^{(1)} = \{\tau_j \in V \mid a_{i,j} = 1, j \neq i\}$ . We first define an anomaly metric:

$$\vartheta(i, t) = \begin{cases} \frac{\mathbf{x}_i(t)}{|\mathcal{N}_i^{(1)}| \sum_{j \in \mathcal{N}_i^{(1)}} \mathbf{x}_j(t)}, & \sum_{j \in \mathcal{N}_i^{(1)}} \mathbf{x}_j(t) \neq 0 \\ \max\{\mathbf{x}_i(t), 1\}, & \sum_{j \in \mathcal{N}_i^{(1)}} \mathbf{x}_j(t) = 0, \end{cases} \quad (8)$$

which is the relative ratio of the data information of city  $i$

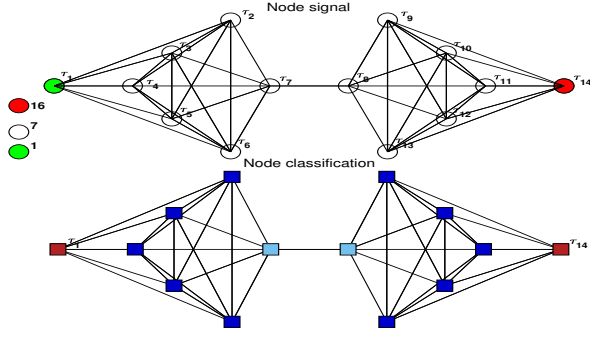


Fig. 12. A specially-designed graph signal function  $f : V \rightarrow \{1, 7, 16\}$ , such that  $f(\tau_1) = 1$  and  $f(\tau_{14}) = 16$ . Both  $\tau_1$  and  $\tau_{14}$  are classified in class  $\mathcal{V}_5$ , even though they are completely different types of outliers.

at time  $t$  compared with the averaging data obtained from its one-hop neighbors.

Then we define the anomaly score (a-score)  $a(i, t)$  to the nodes in the set  $\mathcal{V}_4 \cup \mathcal{V}_5$  according to Fig. 13. According to the a-score, we divide the  $\mathcal{V}_4 \cup \mathcal{V}_5$  into five groups as in Fig. 13.

Classification method	a-score	Groups	Symbols
$\tau_i \in \mathcal{V}_5$ and $\vartheta(i, t) > 1.5$	2	least successful	▲
$\tau_i \in \mathcal{V}_4$ and $\vartheta(i, t) > 1.5$	1	above average	▲
$\tau_i \in \mathcal{V}_4$ and $\vartheta(i, t) < 0.5$	-1	below average	▼
$\tau_i \in \mathcal{V}_5$ and $\vartheta(i, t) < 0.5$	-2	most successful	▼
else	0	others	null

Fig. 13. Refined node classification and a-score in  $\mathcal{V}_4 \cup \mathcal{V}_5$ .

A city with high a-scores presents at risk or volatile in the pandemic. It should ring an alarm for local city administrations, as the city has the potential to increase infection spread to its neighboring cities. Earlier identifying these cities can prevent them from becoming the outbreak cities of a pandemic. On the other hand, identifying cities with low a-scores can be valuable in controlling virus spread, as they provide good models for other cities.

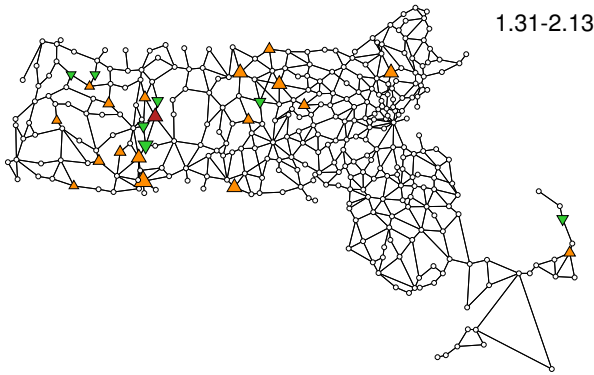


Fig. 14. Refined node classification for the 9th week, from Jan. 31 - Feb. 13.

Fig. 14 depicts the data visualization plots for cities with anomaly patterns from January 31 to February 13. We can quickly detect Amherst with a high a-score, which is also

confirmed as one of the most significant COVID-outbreak cities in Fig. 9.

#### D. Spatio-temporal ranking of super-spreader cities

The a-score defined in Fig. 13 depends on both spatial and temporal coordinates. To have an overall picture of the pandemic evolution behavior of these cities and evaluate the urban pandemic prevention and control, we propose a data visualization plot to explain the level of anomalies by the anomaly score. Below, we use a-scores in Fig. 13, to provide a new city ranking, by taking averages of its a-scores over the 41-week period for each city:

$$\bar{a}(i) := \frac{1}{41} \sum_{t=1}^{41} a(i, t). \quad (9)$$

Fig. 15 shows the average anomaly scores of each city in MA.

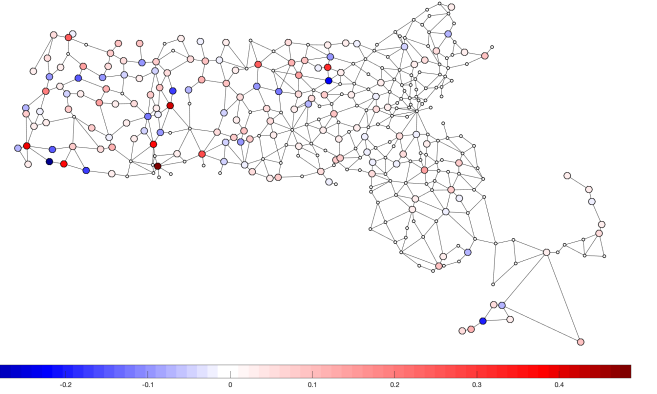


Fig. 15. City spatio-temporal ranking from Dec. 6, 2020 to Sept. 25, 2021, using the average a-score  $\bar{a}$ . Dark red refers to the highest average a-score  $\bar{a}$ , while dark blue refers to the lowest average.

One can see that cities with higher  $\bar{a}(i)$  values are more likely to become super-spreader (cities) for any future pandemic. A by-product of using the  $\bar{a}(i)$  value is that, one could evaluate the city's pandemic prevention and control capabilities. In Fig. 15, the darker the red, the cities have the less successful pandemic prevention and control. On the other hand, the darker the blue, the cities are more successful in pandemic prevention and control. The top five least successful cities are identified as Springfield, Amherst, Great Barrington, Holyoke, and Sandisfield; as well as the top five most successful cities are New Marlborough, Harvard, West Tisbury, Tolland and Leverett.

The detailed visualization analysis for these cities is included in Fig. 16. This visual view can quickly locate the outbreak time and duration of abnormal phenomena. To make effective comparisons, we also plot the pandemic time evolution data of Springfield, Amherst, New Marlborough and Harvard, see Fig. 17 - Fig. 20.

Our analysis identifies Springfield as the least successful city using data from December 6, 2020, to September 25, 2021. Fig. 16 shows that most of the confirmed cases in Springfield surpass the values of the surrounding areas during the entire 41-week period, which can also be confirmed in Fig.

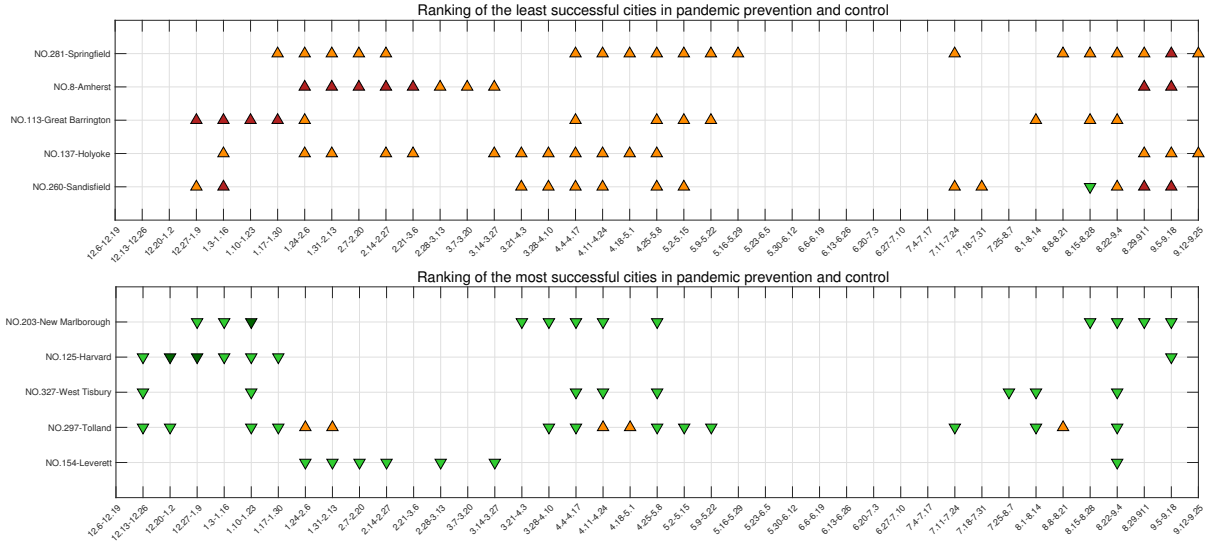


Fig. 16. Ranking of the least successful and most successful cities in pandemic prevention and control from Dec. 16, 2020 to Sept. 25, 2021.

17. A recent report shows that Springfield is a center for the Delta outbreak [23]. This confirms that the city has a much higher risk of spreading new pandemic variants to other cities and may need more help from administrations to control the pandemic.

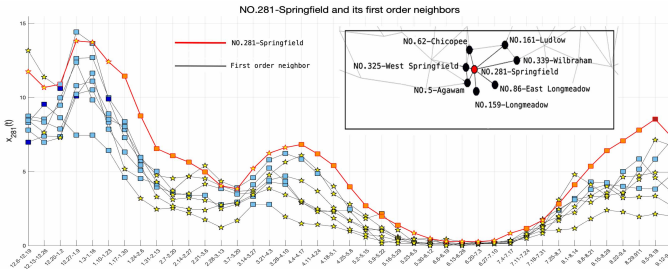


Fig. 17. The 41-week evolution of COVID-19 confirmed cases for Springfield and its neighboring cities from Dec. 19, 2020 to Sept. 25, 2021.

Amherst is ranked as the second least successful city for 41 weeks from December 6, 2020 - September 25, 2021. Fig. 16 indicates that Amherst has much higher confirmed cases than neighbors from January 24 to March 27, 2021, which is consistent with Fig. 18. Indeed, we show that Amherst ranks as the first pandemic spreader during a two-week short periodic from January 31 - February 13, 2021, see Fig. 7. By digging into the news of this period, we find that the University of Massachusetts Amherst started the spring semester on February 1. Because many students moved into dorms or apartments in Amherst, there had been more than 398 active cases during that period. Contact tracing data record [44] has shown that some students failed to follow social distancing and mask protocols in social and residential settings, promoting pandemic virus transmission. Subsequently, the university further strengthened its management standards. For example, students who do not wear masks will not be allowed on campus, and large group gatherings were not encouraged. The pandemic spread was effectively brought under control at the end of February 2021.

At the beginning of the fall semester (the end of August 2021), a similar abnormal situation appeared again in Amherst, see [24], [45].

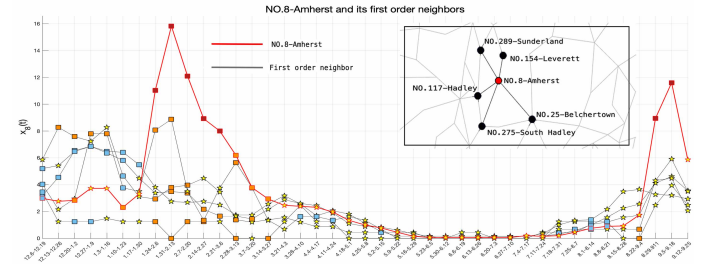


Fig. 18. The 41-week time evolution of COVID-19 confirmed cases for Amherst and its neighboring cities from Dec. 19, 2020 to Sept. 25, 2021.

New Marlborough and Harvard are the top two most successful cities for the 41 weeks from December 6, 2020, to September 25, 2021. Fig. 16 illustrates that the two cities have much lower confirmed cases than those in the surrounding cities most of the time. Fig. 19 and Fig. 20 describe the time

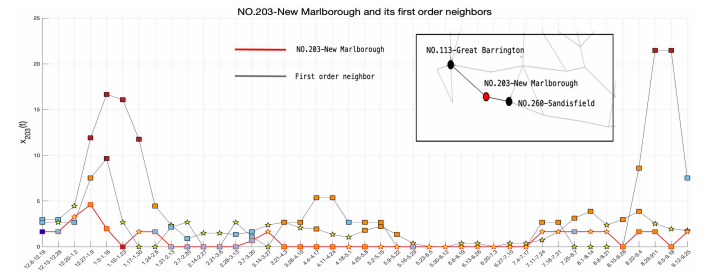


Fig. 19. The 41-week evolution of COVID-19 confirmed cases for New Marlborough and its neighboring cities from Dec. 19, 2020 to Sept. 25, 2021.

evolution of the top two most successful cities, which have good and stable spread patterns during the pandemic, and are consistent with the situation illustrated in Fig. 16. It indicates

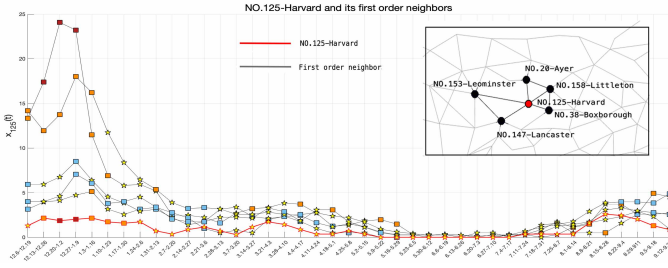


Fig. 20. The 41-week evolution of COVID-19 confirmed cases for Harvard and its neighboring cities from Dec. 19, 2020 to Sept. 25, 2021.

that these cities might have adequate prevention and control measures. By digging into the news of this period, the Health Board in New Marlborough looked for a temporary part-time COVID Ambassador to provide COVID-19 prevention guidance to citizens, businesses and community groups [26], and held several sessions for discussions and updates on COVID-19 [46]. Furthermore, New Marlborough has provided free masks to residents since August 20, 2020 [27]. These measures allow New Marlborough to remain unaffected even when its neighbors sharply all had a sharp increase in cases, see Fig. 19. Harvard offered free safety training courses for workers [28]. Citizens volunteered to help the Board of Health open a local vaccine clinic [29]. These measures may be the reason for the success of Harvard’s pandemic prevention.

In Fig. 16, we show the five most successful and least successful cities. By changing the time range of the formula (9), we can also find successful and least successful cities for any period. As a by-product, our visualization analysis is based on the refined node classification for our spatio-temporal dynamical graph, so it captures correlations of pandemic evolution patterns among these cities. Take Springfield as an example, see Fig. 16. Because the spatio-temporal outbreak patterns of Springfield and Holyoke are similar, we can infer a significant correlation between them. Indeed, we know that they both have large traffic flows and are close to each other, see Fig. 3, thus the patterns of their pandemic outbreaks should be highly related. Our method can quickly help experts locate cities with similar traits and apply insights from a city to inform prevention and control strategies in similar areas.

## VI. CONCLUSION

This paper draws a Massachusetts Route graph based on the latitude and longitude of 351 cities and towns and the main traffic routes passing nearby. The pandemic transition probability is learned through semi-supervised deep learning, based on the Graph Attention Neural Network. We construct a spatio-temporal dynamic model by strong-product for the time-varying data on the graph, which can better capture the spatio-temporal pandemic evolution patterns. With the help of SGWT, the COVID-19 pandemic spread patterns in Massachusetts from December 6, 2020, to September 25, 2021, are analyzed and visualized. In addition to the overall analysis of the temporal and spatial evolution of the pandemic data, we also identify cities with strong pandemic spread influence, such as the town of Otis. We also construct a new anomaly

indicator to classify cities with abnormal pandemic situations, indicating cities at risk of virus transmission, and identifying cities that are likely to be infected in the next step. The five cities identified with the least successful pandemic prevention are Springfield, Amherst, Great Barrington, Holyoke, and Sandisfield; the five cities with the most successful pandemic prevention are New Marlborough, Harvard, West Tisbury, Tolland, and Leverett. These obtained results not only offer descriptive insight for strategizing purposes in combating the COVID-19 outbreak in Massachusetts, but also can be used to protect those high-risk cities for the next possible round of pandemics. Further, it also provides a framework for evaluating regional pandemic prevention work in the COVID-19 pandemic. It helps the policymakers identify cities with better prevention in the pandemic and extract insights from the successes.

However, in this paper, we only analyze cities and towns within Massachusetts and do not consider the impact on other states. In our further study, we will take our focus on the influence of neighboring states to improve our method. In addition, when calculating the transition probability matrix using GAT, due to the limited features of our data, we take the time series of confirmed cases every two weeks and obtain the transition probability of the comprehensive pandemic evolution for 41 weeks. Our further research will try to overcome the limited features of the data and train the network on the spatio-temporal dynamic graph to obtain the time-varying transition probability matrix.

## CONFLICT OF INTEREST

The authors declare that they have no conflict of interest.

## APPENDIX

### LIST OF MASSACHUSETTS CITIES

### REFERENCES

- [1] World Health Organization, “WHO director-general’s opening remarks at the media briefing on COVID-19 - 11 march 2020,” <https://www.who.int/director-general/speeches/detail/who-director-general-s-opening-remarks-at-the-media-briefing-on-covid-19---11-march-2020>, Mar. 11, 2020 [Online].
- [2] Johns Hopkins Coronavirus Resource Center, “COVID-19 dashboard,” <https://coronavirus.jhu.edu/map.html>, Dec. 1, 2021 [Online].
- [3] Q. Gao, J. Zhuang, T. Wu, and H. Shen, “Transmission dynamics and quarantine control of covid-19 in cluster community: A new transmission-quarantine model with case study for diamond princess,” *Mathematical Models and Methods in Applied Sciences*, vol. 31, no. 03, pp. 619–648, 2021.
- [4] K. E. Church, “Analysis of pandemic closing-reopening cycles using rigorous homotopy continuation: a case study with montreal COVID-19 data,” *SIAM Journal on Applied Dynamical Systems*, vol. 20, no. 2, pp. 745–783, 2021.
- [5] A. G. Neves and G. Guerrero, “Predicting the evolution of the COVID-19 epidemic with the a-sir model: Lombardy, italy and sao paulo state, brazil,” *Physica D: Nonlinear Phenomena*, vol. 413, p. 132693, 2020.
- [6] K. Y. Ng and M. M. Gui, “COVID-19: development of a robust mathematical model and simulation package with consideration for ageing population and time delay for control action and resusceptibility,” *Physica D: Nonlinear Phenomena*, vol. 411, p. 132599, 2020.
- [7] J. G. V. Miranda, M. S. Silva, J. G. Bertolino, R. N. Vasconcelos, E. C. B. Cambui, M. L. V. Araújo, H. Saba, D. P. Costa, S. G. Duverger, M. T. de Oliveira *et al.*, “Scaling effect in COVID-19 spreading: The role of heterogeneity in a hybrid ode-network model with restrictions on the inter-cities flow,” *Physica D: Nonlinear Phenomena*, vol. 415, p. 132792, 2021.



TABLE II  
LIST OF MASSACHUSETTS CITIES

ID	City/Town	ID	City/Town	ID	City/Town	ID	City/Town	ID	City/Town
1	Abington	70	Cummington	142	Hull	215	Northborough	283	Stockbridge
2	Acton	71	Dalton	143	Huntington	216	Northbridge	284	Stoneham
3	Acushnet	72	Danvers	144	Ipswich	217	Northfield	285	Stoughton
4	Adams	73	Dartmouth	145	Kingston	218	Norton	286	Stow
5	Agawam	74	Dedham	146	Lakeville	219	Norwell	287	Sturbridge
7	Amesbury	75	Deerfield	147	Lancaster	220	Norwood	288	Sudbury
8	Amherst	76	Dennis	148	Lanesborough	221	Oak Bluffs	289	Sunderland
9	Andover	77	Dighton	149	Lawrence	222	Oakham	290	Sutton
10	Aquinnah	78	Douglas	150	Lee	223	Orange	291	Swampscott
11	Arlington	80	Dracut	151	Leicester	224	Orleans	292	Swansea
12	Ashburnham	81	Dudley	152	Lenox	225	Otis	293	Taunton
13	Ashby	82	Dunstable	153	Leominster	226	Oxford	294	Templeton
14	Ashfield	83	Duxbury	154	Leverett	227	Palmer	295	Tewksbury
15	Ashland	84	East Bridgewater	155	Lexington	228	Paxton	296	Tisbury
16	Athol	85	East Brookfield	157	Lincoln	229	Peabody	297	Tolland
17	Attleboro	86	East Longmeadow	158	Littleton	230	Pelham	298	Topsfield
18	Auburn	87	Eastham	159	Longmeadow	231	Pembroke	299	Townsend
19	Avon	88	Easthampton	160	Lowell	232	Pepperell	300	Truro
20	Ayer	89	Easton	161	Ludlow	233	Peru	301	Tyngsborough
21	Barnstable	90	Edgartown	162	Lunenburg	234	Petersham	303	Upton
22	Barre	91	Egremont	163	Lynn	235	Phillipston	304	Uxbridge
23	Becket	92	Erving	164	Lynnfield	236	Pittsfield	305	Wakefield
24	Bedford	93	Essex	165	Malden	237	Plainfield	306	Wales
25	Belchertown	94	Everett	166	Manchester	238	Plainville	307	Walpole
26	Bellingham	95	Fairhaven	167	Mansfield	239	Plymouth	308	Waltham
27	Belmont	96	Fall River	168	Marblehead	240	Plympton	309	Ware
28	Berkley	97	Falmouth	169	Marion	241	Princeton	310	Wareham
29	Berlin	98	Fitchburg	170	Marlborough	242	Provincetown	311	Warren
30	Bernardston	99	Florida	171	Marshfield	243	Quincy	312	Warwick
31	Beverly	100	Foxborough	172	Mashpee	244	Randolph	313	Washington
32	Billerica	101	Framingham	173	Mattapoisett	245	Raynham	314	Watertown
33	Blackstone	102	Franklin	174	Maynard	246	Reading	315	Wayland
34	Blandford	103	Freetown	175	Medfield	247	Rehoboth	316	Webster
35	Bolton	104	Gardner	176	Medford	248	Revere	317	Wellesley
36	Boston	105	Georgetown	177	Medway	249	Richmond	318	Wellfleet
37	Bourne	106	Gill	178	Melrose	250	Rochester	320	Wenham
38	Boxborough	107	Gloucester	179	Mendon	251	Rockland	321	West Boylston
39	Boxford	108	Goshen	180	Merrimac	252	Rockport	322	West Bridgewater
40	Boylston	110	Grafton	181	Methuen	254	Rowley	323	West Brookfield
41	Braintree	111	Granby	182	Middleborough	255	Royalston	324	West Newbury
42	Brewster	112	Granville	184	Middleton	256	Russell	325	West Springfield
43	Bridgewater	113	Great Barrington	185	Milford	257	Rutland	326	West Stockbridge
44	Brimfield	114	Greenfield	186	Millbury	258	Salem	327	West Tisbury
45	Brockton	115	Groton	187	Millis	259	Salisbury	328	Westborough
46	Brookfield	116	Groveland	188	Millville	260	Sandisfield	329	Westfield
47	Brookline	117	Hadley	189	Milton	261	Sandwich	330	Westford
48	Buckland	118	Halifax	191	Monson	262	Saugus	331	Westhampton
49	Burlington	119	Hamilton	192	Montague	263	Savoy	332	Westminster
50	Cambridge	121	Hancock	193	Monterey	264	Scituate	333	Weston
51	Canton	122	Hanover	196	Nahant	265	Seekonk	334	Westport
52	Carlisle	123	Hanson	197	Nantucket	266	Sharon	335	Westwood
53	Carver	124	Hardwick	198	Natick	267	Sheffield	336	Weymouth
54	Charlemont	125	Harvard	199	Needham	268	Shelburne	337	Whately
55	Charlton	126	Harwich	200	New Ashford	269	Sherborn	338	Whitman
56	Chatham	127	Hatfield	201	New Bedford	270	Shirley	339	Wilbraham
57	Chelmsford	128	Haverhill	202	New Braintree	271	Shrewsbury	340	Williamsburg
58	Chelsea	129	Hawley	203	New Marlborough	272	Shutesbury	341	Williamstown
59	Cheshire	130	Heath	204	New Salem	273	Somerset	342	Wilmington
60	Chester	131	Hingham	205	Newbury	274	Somerville	343	Winchendon
61	Chesterfield	132	Hinsdale	206	Newburyport	275	South Hadley	344	Winchester
62	Chicopee	133	Holbrook	207	Newton	276	Southampton	345	Windsor
63	Chilmark	134	Holden	208	Norfolk	277	Southborough	346	Winthrop
64	Clarksburg	136	Holliston	209	North Adams	278	Southbridge	347	Woburn
65	Clinton	137	Holyoke	210	North Andover	279	Southwick	348	Worcester
66	Cohasset	138	Hopedale	211	North Attleborough	280	Spencer	349	Worthington
67	Colrain	139	Hopkinton	212	North Brookfield	281	Springfield	350	Wrentham
68	Concord	140	Hubbardston	213	North Reading	282	Sterling	351	Yarmouth
69	Conway	141	Hudson	214	Northampton				
Thirteen isolated cities									
6	Alford	79	Dover	109	Gosnold	120	Hampden	135	Holland
156	Leyden	183	Middlefield	190	Monroe	194	Montgomery	195	Mount Washington
253	Rowe	302	Tyringham	319	Wendell				



- [8] F. Tang, Y. Feng, H. Chiheb, and J. Fan, "The interplay of demographic variables and social distancing scores in deep prediction of US COVID-19 cases," *Journal of the American Statistical Association*, vol. 116, no. 534, pp. 492–506, 2021.
- [9] P. Melin, J. C. Monica, D. Sanchez, and O. Castillo, "Analysis of spatial spread relationships of coronavirus (COVID-19) pandemic in the world using self organizing maps," *Chaos Solitons and Fractals*, vol. 138, p. 109917, 2020.
- [10] T. Tat Dat, P. Frédéric, N. T. Hang, M. Jules, N. Duc Thang, C. Piffault, R. Willy, F. Susely, H. V. Lê, W. Tuschmann *et al.*, "Epidemic dynamics via wavelet theory and machine learning with applications to COVID-19," *Biology*, vol. 9, no. 12, p. 477, 2020.
- [11] Y. Li and G. Mateos, "Graph frequency analysis of COVID-19 incidence to identify county-level contagion patterns in the United States," in *ICASSP 2021-2021 IEEE International Conference on Acoustics, Speech and Signal Processing (ICASSP)*. IEEE, 2021, pp. 3230–3234.
- [12] J. Gao, R. Sharma, C. Qian, L. M. Glass, J. Spaeder, J. Romberg, J. Sun, and C. Xiao, "STAN: spatio-temporal attention network for pandemic prediction using real-world evidence," *Journal of the American Medical Informatics Association*, vol. 28, no. 4, pp. 733–743, 2021.
- [13] A. Kapoor, X. Ben, L. Liu, B. Perozzi, M. Barnes, M. Blais, and S. O'Banion, "Examining COVID-19 forecasting using spatio-temporal graph neural networks," *arXiv preprint arXiv:2007.03113*, 2020.
- [14] P. Veličković, G. Cucurull, A. Casanova, A. Romero, P. Liò, and Y. Bengio, "Graph attention networks," in *International Conference on Learning Representations*, 2018.
- [15] W. Gu, F. Gao, X. Lou, and J. Zhang, "Link prediction via graph attention network," *arXiv preprint arXiv:1910.04807*, 2019.
- [16] C. Tang, J. Sun, Y. Sun, M. Peng, and N. Gan, "A general traffic flow prediction approach based on spatial-temporal graph attention," *IEEE Access*, vol. 8, pp. 153 731–153 741, 2020.
- [17] H. Zhou, D. Ren, H. Xia, M. Fan, X. Yang, and H. Huang, "AST-GNN: An attention-based spatio-temporal graph neural network for interaction-aware pedestrian trajectory prediction," *Neurocomputing*, vol. 445, pp. 298–308, 2021.
- [18] Z. Zhang, J. Huang, and Q. Tan, "SR-HGAT: Symmetric relations based heterogeneous graph attention network," *IEEE Access*, vol. 8, pp. 165 631–165 645, 2020.
- [19] A. Vaswani, N. Shazeer, N. Parmar, J. Uszkoreit, L. Jones, A. N. Gomez, E. Kaiser, and I. Polosukhin, "Attention is all you need," in *Advances in neural information processing systems*, 2017, pp. 5998–6008.
- [20] R. H. Hammack, W. Imrich, S. Klavžar, W. Imrich, and S. Klavžar, *Handbook of product graphs*. CRC press Boca Raton, 2011, vol. 2.
- [21] D. K. Hammond, P. Vandergheynst, and R. Gribonval, "Wavelets on graphs via spectral graph theory," *Applied and Computational Harmonic Analysis*, vol. 30, no. 2, pp. 129–150, 2011.
- [22] D. I. Shuman, C. Wiesmeyr, N. Holighaus, and P. Vandergheynst, "Spectrum-adapted tight graph wavelet and vertex-frequency frames," *IEEE Transactions on Signal Processing*, vol. 63, no. 16, pp. 4223–4235, 2015.
- [23] E. Kuschel and B. Strohl, "COVID-19 hospitalizations in the Ozarks near pre-delta variant numbers," <https://www.ozarksfirst.com/local-news/local-news-local-news/covid-19-hospitalizations-in-the-ozarks-near-pre-delta-variant-numbers/>, Sep. 15, 2021 [Online].
- [24] K. Wilkinson, "Over 100 breakthrough COVID-19 cases reported at UMass Amherst," <https://www.wvlp.com/news/local-news/hampshire-county/over-100-breakthrough-covid-19-cases-reported-at-umass-amherst/>, Sep. 9, 2021 [Online].
- [25] M. Rosenfield, "'Preventable Tragedy': Committee issues report on COVID deaths at Holyoke soldiers' home," <https://www.nbcboston.com/news/coronavirus/preventable-tragedy-mass-committee-issues-report-on-covid-deaths-at-holyoke-soldiers-home/2389122/>, May. 24, 2021 [Online].
- [26] Marlborough-ma.gov, "Position available – COVID ambassador – PT, temporary," [https://www.marlbrough-ma.gov/sites/g/files/vyhlf7576/f/uploads/aa20-24\\_boh\\_covid\\_ambassador\\_pt\\_temp\\_0.pdf](https://www.marlbrough-ma.gov/sites/g/files/vyhlf7576/f/uploads/aa20-24_boh_covid_ambassador_pt_temp_0.pdf), 2020 [Online].
- [27] —, "Marlborough COVID-19 city updates," [https://www.marlbrough-ma.gov/sites/g/files/vyhlf7576/f/news/marlborough\\_covid-19\\_8.20.pdf](https://www.marlbrough-ma.gov/sites/g/files/vyhlf7576/f/news/marlborough_covid-19_8.20.pdf), Aug. 20, 2020 [Online].
- [28] Harvard-ma.gov, "COVID-19 pandemic: Next steps for worker safety as organizations open during COVID-19," [https://www.harvard-ma.gov/sites/g/files/vyhlf676/f/uploads/tnc\\_r\\_eopening\\_business\\_during\\_covid\\_october\\_2020\\_flyer.pdf](https://www.harvard-ma.gov/sites/g/files/vyhlf676/f/uploads/tnc_r_eopening_business_during_covid_october_2020_flyer.pdf), Oct., 2020 [Online].
- [29] —, "Harvard BOH update on local COVID-19 vaccination clinics," <https://www.harvard-ma.gov/board-health/news/harvard-boh-update-local-covid-19-vaccination-clinics>, Feb. 24, 2021 [Online].
- [30] J. Chesak, "Which cities and states have had the best COVID-19 response?" <https://www.verywellhealth.com/covid-19-response-city-state-response-5086171>, Nov. 8, 2020 [Online].
- [31] Massachusetts Department of Public Health, "Archive of COVID-19 cases in Massachusetts," <https://www.mass.gov/info-details/archive-of-covid-19-cases-in-massachusetts>, Nov., 2021 [Online].
- [32] Geohack.toolforge.org, <https://geohack.toolforge.org>, 2021 [Online].
- [33] N. Vaishnav and A. Tatu, "A graph downsampling technique based on graph fourier transform," *arXiv preprint arXiv:1612.07542*, 2016.
- [34] T. Nguyen, M. Raghu, and S. Kornblith, "Do wide and deep networks learn the same things? uncovering how neural network representations vary with width and depth," *arXiv preprint arXiv:2010.15327*, 2020.
- [35] A. Sandryhaila and J. Moura, "Big data analysis with signal processing on graphs: Representation and processing of massive data sets with irregular structure," *IEEE Signal Processing Magazine*, vol. 31, no. 5, pp. 80–90, 2014.
- [36] P. Valdivia, F. Dias, F. Petronetto, C. T. Silva, and L. G. Nonato, "Wavelet-based visualization of time-varying data on graphs," in *2015 IEEE Conference on Visual Analytics Science and Technology (VAST)*. IEEE, 2015, pp. 1–8.
- [37] A. Dal Col, P. Valdivia, F. Petronetto, F. Dias, C. T. Silva, and L. G. Nonato, "Wavelet-based visual analysis for data exploration," *Computing in Science Engineering*, vol. 19, no. 5, pp. 85–91, 2017.
- [38] A. Dal Col, P. Valdivia, F. Petronetto, F. Dias, C. T. Silva, and L. G. Nonato, "Wavelet-based visual analysis of dynamic networks," *IEEE Transactions on Visualization and Computer Graphics*, vol. 24, no. 8, pp. 2456–2469, 2018.
- [39] D. I. Shuman, P. Vandergheynst, D. Kressner, and P. Frossard, "Distributed signal processing via chebyshev polynomial approximation," *IEEE Transactions on Signal and Information Processing over Networks*, vol. 4, no. 4, pp. 736–751, 2018.
- [40] B. A. Keen, "Feature scaling with scikit-learn," <https://benalexkeen.com/feature-scaling-with-scikit-learn/>, May. 10, 2017 [Online].
- [41] H. Yao, C. Jiang, and Y. Qian, *Developing networks using artificial intelligence*. Springer, 2019.
- [42] UMass Amherst COVID-19 Information, "All UMass athletic activities on pause," <https://www.umass.edu/coronavirus/news/all-umass-athletic-activities-pause>, Feb. 7, 2021 [Online].
- [43] W. Katcher, "In areas with highest COVID rates, Amherst leads Massachusetts communities over 10,000 people; see how your town compared," <https://www.masslive.com/news/2021/09/in-areas-with-highest-covid-rates-amherst-leads-massachusetts-communities-over-10000-people-see-how-your-town-compared.html>, Sep. 17, 2021 [Online].
- [44] UMass Amherst COVID-19 Information, "Campus COVID-19 risk level raised from 'elevated' to 'high' risk," <https://www.umass.edu/coronavirus/campus-covid-19-risk-level-raised-elevated-high-risk>, Feb. 7, 2021 [Online].
- [45] AMHERSTMA.GOV - NEWS, "Town of Amherst COVID-19 update - September 10, 2021," <https://www.amherstma.gov/CivicAlerts.aspx?AID=2966&ARC=5832>, Sep. 10, 2021 [Online].
- [46] Marlborough-ma.gov, "Board of health meeting agenda," <https://www.marlbrough-ma.gov/board-health/agenda/board-health-meeting-agenda-5>, Nov. 9, 2020 [Online].